The Astrophysical Journal Letters, 990:L58 (5pp), 2025 September 10 https://doi.org/10.3847/2041-8213/adfec6

Euclid and Roman with JWST Could Reveal Supermassive Black Holes at up to $z \sim 15$

Muhammad A. Latif[1] and Daniel J. Whalen[2]
[1] Physics Department, College of Science, United Arab Emirates University, PO Box 15551, Al-Ain, UAE; latifne@gmail.com
[2] Institute of Cosmology and Gravitation, Portsmouth University, Dennis Sciama Building, Portsmouth PO1 3FX, UK
Received 2025 June 20; revised 2025 August 20; accepted 2025 August 22; published 2025 September 8

Abstract

Although supermassive black holes (SMBHs) are found at the centers of most galaxies today, over 300 have now been discovered at $z > 6$, including UHZ1 at $z = 10.1$ and GHZ9 at $z = 10.4$. They are thought to form when 10^4 to 10^5 $M_\odot$ primordial stars die as direct-collapse black holes (DCBHs) at $z \sim 20$–25. While studies have shown that DCBHs should be visible at birth at $z \gtrsim 20$ in the near-infrared (NIR) to the James Webb Space Telescope (JWST), none have considered SMBH detections at later stages of growth down to $z \sim 6$–7. Here, we present continuum NIR luminosities for a black hole (BH) like ULAS J1120+0641, a 1.35×10^9 $M_\odot$ quasar at $z = 7.1$, from a cosmological simulation for Euclid, Roman Space Telescope (RST), and JWST bands from $z = 6$ to 15. We find that Euclid and RST could detect such BHs, including others like UHZ1 and GHZ9, at much earlier stages of evolution, out to $z \sim 14$–15, and that their redshifts could be confirmed spectroscopically with JWST. Synergies between these three telescopes could thus reveal the numbers of SMBHs at much higher redshifts and discriminate between their evolution pathways because Euclid and RST can capture large numbers of them in wide-field surveys for further study by JWST.

Unified Astronomy Thesaurus concepts: Quasars (1319); Supermassive black holes (1663)

1. Introduction

Supermassive black holes (SMBHs) at $z > 6$ were first detected in the Sloan Digital Sky Survey over 20 yr ago (X. Fan et al. 2003). Since then, their numbers have risen to over 300, with 13 at $z > 7$ (D. J. Mortlock et al. 2011; E. Bañados et al. 2018; J. Yang et al. 2020; F. Wang et al. 2021). A new class of active galactic nuclei (AGNs) has now been found at even higher redshifts, such as a 4×10^7 $M_\odot$ black hole (BH) in UHZ1 at $z = 10.1$ (Á. Bogdán et al. 2024; M. Castellano et al. 2023; A. D. Goulding et al. 2023) and an 8×10^7 $M_\odot$ BH in GHZ9 at $z = 10.4$ (H. Atek et al. 2023; M. Castellano et al. 2023; O. E. Kovács et al. 2024). In principle, low-mass Population III (Pop III) stars could be the seeds of these BHs if they accrete continuously at the Eddington limit or grow by super-Eddington accretion (M. Volonteri et al. 2015; K. Inayoshi et al. 2016; A. Lupi et al. 2024). However, this scenario is problematic because Pop III BHs are born in low densities that preclude rapid initial growth (e.g., T. Kitayama et al. 2004; D. Whalen et al. 2004; M. A. Latif et al. 2022a), and they can be ejected from their host halos during collapse (D. J. Whalen & C. L. Fryer 2012). When they do accrete, they drive gas out of their halos because of their shallow gravitational potential wells, so they are restricted to fairly low duty cycles (B. D. Smith et al. 2018).

It is generally thought that the $z > 6$ quasars grew from direct-collapse black holes (DCBHs) that form and then rapidly grow in the low-shear environments of rare, massive halos fed by strong accretion flows (B. D. Smith et al. 2018; A. Tenneti et al. 2018; A. Lupi et al. 2021; M. Valentini et al. 2021). The highly supersonic turbulence in these unusual halos produces supermassive stars (SMSs; T. Hosokawa et al. 2013; T. E. Woods et al. 2017; L. Haemmerlé et al. 2018; T. E. Woods et al. 2021; N. P. Herrington et al. 2023; D. Nandal et al. 2024b) without any need for exotic environments (or even atomic cooling, as had been supposed for nearly 20 yr; M. A. Latif et al. 2022b). DCBHs grow at much higher rates than Pop III BHs because Bondi–Hoyle accretion rates scale as $M_{\rm BH}^2$, and they form in much higher densities (e.g., S. J. Patrick et al. 2023) in more massive halos that retain gas even when it is photoionized by X-rays (T. E. Woods et al. 2019; M. A. Latif et al. 2021). SMSs are also probably required to explain the large nitrogen excesses in GN-z11 (A. J. Bunker et al. 2023; P. Senchyna et al. 2024), CEERS 1019 (R. L. Larson et al. 2023), and GS 3073 (X. Ji et al. 2024), high-redshift galaxies at $z \sim 5.5$–10.5 (C. Nagele et al. 2023a; D. Nandal et al. 2024a, 2025).

SMSs can be detected in the near-infrared (NIR) at $z \sim 8$–14 (M. Surace et al. 2018, 2019; A. Vikaeus et al. 2022; C. Nagele et al. 2023b), and DCBHs can be found at $z \gtrsim 20$ by JWST (P. Natarajan et al. 2017; K. S. S. Barrow et al. 2018; D. J. Whalen et al. 2020b) and at $z \sim 8$–10 by the Square Kilometer Array (SKA) and next-generation Very Large Array (ngVLA; D. J. Whalen et al. 2020a, 2021). Quasars like ULAS J1120+0641, a 1.35×10^9 $M_\odot$ BH at $z = 7.1$ that is typical of $z \sim 6$–7 SMBHs, can be detected at much earlier stages of evolution ($z \sim 14$–15) at 0.1–10 GHz, but only in blind surveys that may not yield many objects because of these telescopes' small fields of view (D. J. Whalen et al. 2023; M. A. Latif et al. 2024a, 2024b, 2025; M. A. Latif & D. J. Whalen 2025).

However, Euclid and the Roman Space Telescope (RST) could in principle photometrically identify much larger numbers of SMBHs at $z > 6$–7 because of their large survey areas. Once found, their properties and redshifts could be determined spectroscopically by JWST. Observations of SMBHs at earlier stages of evolution at $z > 7$ are clearly needed to determine their numbers and probe their formation pathways. We have calculated NIR luminosities for a quasar like J1120 at earlier stages of evolution, $z = 6$–15, to

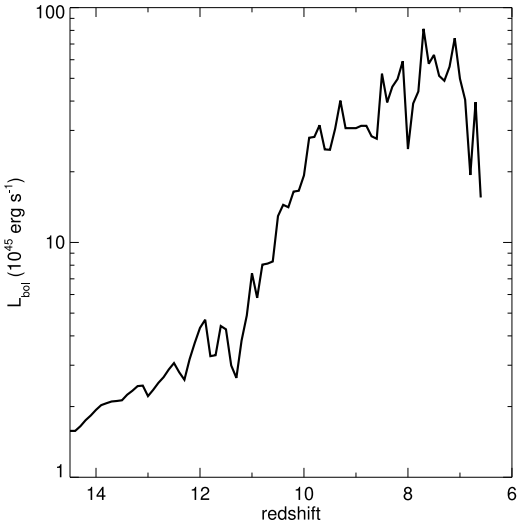

Figure 1. Bolometric luminosities, $L_{\rm bol}$, for the quasar as a function of redshift from J. Smidt et al. (2018).

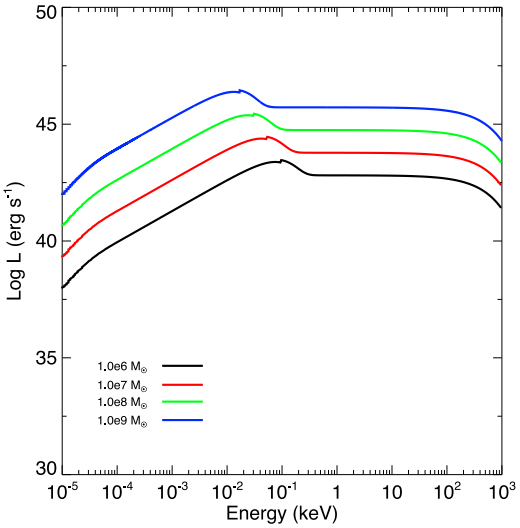

Figure 2. Rest-frame quasar spectra at 10^6, 10^7, 10^8, and 10^9 $M_\odot$, shown by the black, red, green and blue lines, respectively.

determine at what redshifts it could be found by Euclid, RST, and JWST. In Section 2 we describe our NIR AB magnitude estimates. We discuss AB mag limits for the quasar in redshift for all three telescopes in Section 3.

2. Numerical Method

We first calculate rest-frame spectra for our fiducial quasar by normalizing theoretical spectra for BH accretion disks from B. Yue et al. (2013) to bolometric luminosities for the quasar in the cosmological simulation by J. Smidt et al. (2018). This simulation used radiation hydrodynamics to model X-ray feedback from the BH and ionizing UV from stars in the host galaxy along with local supernova feedback and chemical enrichment due to massive stars. It produced a quasar with the same mass and star formation rate as in J1120 at $z = 7.1$. We utilize the data from this simulation to compute spectra and then cosmologically dim and redshift these spectra and convolve them with Euclid, RST, and JWST filter functions to obtain AB magnitudes. Bolometric luminosities, $L_{\rm bol}$, for the quasar are shown for $z =$ 6–14.5 in Figure 1. Masses and accretion rates for the BH are shown in Figure 2 of J. Smidt et al. (2018). They vary from 10^6 to 10^9 $M_\odot$ and 0.01–20 $M_\odot$ yr^{-1} ($\sim$0.2–0.8 $\dot{M}_{\rm Edd}$) from $z = 15$ to 7. At these rates the disk is expected to be thin, Compton-thick, and radiatively efficient, so the spectral luminosity can be modeled as the sum of three components (B. Yue et al. 2013),

$$L_\nu = L_\nu^{\rm MBB} + L_\nu^{\rm PL} + L_\nu^{\rm refl}, \quad (1)$$

a multicolor blackbody part due to the range of temperatures across the disk, a power-law component from the surrounding hot corona, and a reflection component, respectively. We omit the contribution due to reflection because it is at most 10% of the entire spectrum and is at energies well above those redshifted into the NIR today.

The temperature of the BH accretion disk is highest at its center, where

$$T_{\rm max} = \left(\frac{M_{\rm BH}}{M_\odot}\right)^{-0.25} {\rm keV}, \quad (2)$$

and decreases at larger radii (K. Makishima et al. 2000; R. Salvaterra et al. 2005). As the SMBH grows from 10^6 to 10^9 $M_\odot$, temperatures at the center of the disk fall from $\sim$600,000 to 60,000 K. Equation (2) is valid if the central engine is a Schwarzschild BH, the innermost radius is about 5 times the Schwarzschild radius, and the accretion is at or near the Eddington limit. The spectral luminosity is then

$$L_\nu^{\rm MBB} = L_{\rm MBB} \int_0^{T_{\rm max}} B_\nu(T) \left(\frac{T}{T_{\rm max}}\right)^{-11/3} \frac{dT}{T_{\rm max}}, \quad (3)$$

where $B_\nu(T)$ is the emission spectrum of a blackbody with temperature T and $L_{\rm MBB}$ is a normalization factor.

As in B. Yue et al. (2013), we parameterize the emission spectrum of the hot corona as a power law with an exponential cutoff:

$$L_\nu^{\rm PL} = L_{\rm PL}\, \nu^{\alpha_{\rm s}} \exp(-h\nu/E_{\rm cut}), \quad (4)$$

where we set $\alpha_{\rm s} = 1$, $E_{\rm cut} = 300$ keV (S. Y. Sazonov et al. 2004), and $L_{\rm PL}$ is a normalization factor. As in R. Salvaterra et al. (2005) and B. Yue et al. (2013), we truncate the power law below the peak of the disk component, at $\sim$3 $T_{\rm max}$.

We estimate normalization factors $L_{\rm MBB}$ and $L_{\rm PL}$ by setting

$$\int (L_\nu^{\rm MBB} + L_\nu^{\rm PL}) d\nu = L_{\rm bol}. \quad (5)$$

Following B. Yue et al. (2013), this then leads to

$$L_{\rm MBB} = 0.5\, L_{\rm bol} / \int L_\nu^{\rm MBB} d\nu \quad (6)$$

and

$$L_{\rm PL} = 0.5\, L_{\rm bol} / \int L_\nu^{\rm PL} d\nu. \quad (7)$$

We show spectra at 10^{-5}–10^3 keV over 4 decades in BH mass, 10^6–10^9 $M_\odot$, in Figure 2. As the mass increases, the spectral peak shifts to lower energies, resulting in a softening of the quasar spectrum. This is consistent with the decrease in $T_{\rm max}$ by about an order of magnitude over this range. However, the slope of the spectrum is nearly constant over the interval in energy that is redshifted into the NIR bands we consider.

3. Results

We show AB magnitudes for the quasar at $z = 6$–14.5 in the Euclid H and J bands and the RST H, J, and Y bands in the top and center panels of Figure 3 (although we note that RST could detect SMBHs out to $z \sim 18$ because its F213 filter extends down to 2.30 μm, unlike Euclid's H-band filter, which cuts off at 2.0 μm and would limit detections to $z \sim 15.5$). We superimpose detection limits for the 15,000 deg^2 Euclid Wide Survey (WS; 24.5 AB mag; Euclid Collaboration et al. 2025), the 50 deg^2 Deep Survey (DS; 26.0 AB mag), and the $\sim$1 deg^2 Euclid Ultra Deep Survey (EUDS; 27.7 AB mag) on the top panel and for the 2000 deg^2 RST High Latitute Spectroscopic Survey (HLSS; 28 AB mag; Y. Wang et al. 2022) in the middle panel. The Euclid WS could photometrically detect a quasar like J1120 at redshifts up to $z \sim 11$, while the DS and EUDS could detect them out to $z \sim 13$ and $z \sim 14$, respectively, when the BH only has a mass of $\sim 10^6\ M_\odot$ and an accretion rate of $\sim$0.8 $\dot{M}_{\rm Edd}$ (see Figures 2 and 3 of J. Smidt et al. 2018). These are effectively the upper limits in z for detection by Euclid because photons redshifted into the H- and Y-band filters from earlier times would be blueward of the Lyman limit in the rest frame and be resonantly scattered or absorbed by the neutral intergalactic medium.

In contrast, RST could detect this quasar at $z \lesssim 14.5$ in the H, J, and Y filters, making it the observatory of choice for initial detection of quasars at earlier times because of its high sensitivities and large survey areas. We show AB magnitudes in the 2.50 μm, 3.56 μm, 4.44 μm, and 4.60 μm JWST NIRCam filters in the bottom panel of Figure 3. They are well above NIRCam detection limits ($\sim$ AB mag 32, not visible in the plot), or even NIRSpec limits, $\sim$29 at $z \lesssim 15$. JWST could thus spectroscopically confirm redshifts of BHs with masses as low as $\sim 10^6\ M_\odot$ if they accrete at or about the Eddington limit at $z \sim 15$. M. Castellano et al. (2023) reported NIR AB magnitudes of 26.2 for UHZ1 and 27.1 for GHZ9 in the JWST F200 filters, so the Euclid Deep and Ultra Deep Surveys could detect UHZ1 and the RST HLSS could detect either object at their respective redshifts. Since the inferred masses of these two BHs are $\sim 10^7\ M_\odot$ and $7 \times 10^7\ M_\odot$, respectively, our NIR magnitudes indicate that they also could have been detected at earlier stages of growth at masses $\gtrsim 10^6\ M_\odot$, likely out to $z \sim 15$.

Predictions of early quasar counts in survey fields depend on their number densities at high redshift, which are uncertain, and survey depth. On the low end, large-scale cosmological simulations dedicated to high-z BH growth indicate that there are about a dozen gas reservoirs per Gpc^3 that are capable of hosting $10^9\ M_\odot$ quasars by $z \sim 7$ (e.g., T. Di Matteo et al. 2012, 2017). On the high end, predictions of DCBH number densities vary from 10^{-5} to 10^{-8} Mpc^{-3} at $z = 10$–15, depending on the strength of UV backgrounds (M. Habouzit et al. 2016; H. O'Brennan et al. 2025), so clearly not all of them are destined to become quasars because their growth is quenched at some point. Most will instead become less luminous AGNs such as the "little red dots" (A. D. Goulding et al. 2023; D. D. Kocevski et al. 2025).

We show the expected numbers of BH detections in the Euclid Wide Survey, Euclid Deep Survey (EDS), and HLSS in Figure 4 based on predicted numbers of DCBHs from simulations as a function of redshift (M. Habouzit et al. 2016) and for the JWST AGN luminosity function (V. Kokorev et al. 2024; K. Inayoshi 2025; D. D. Kocevski et al. 2025)

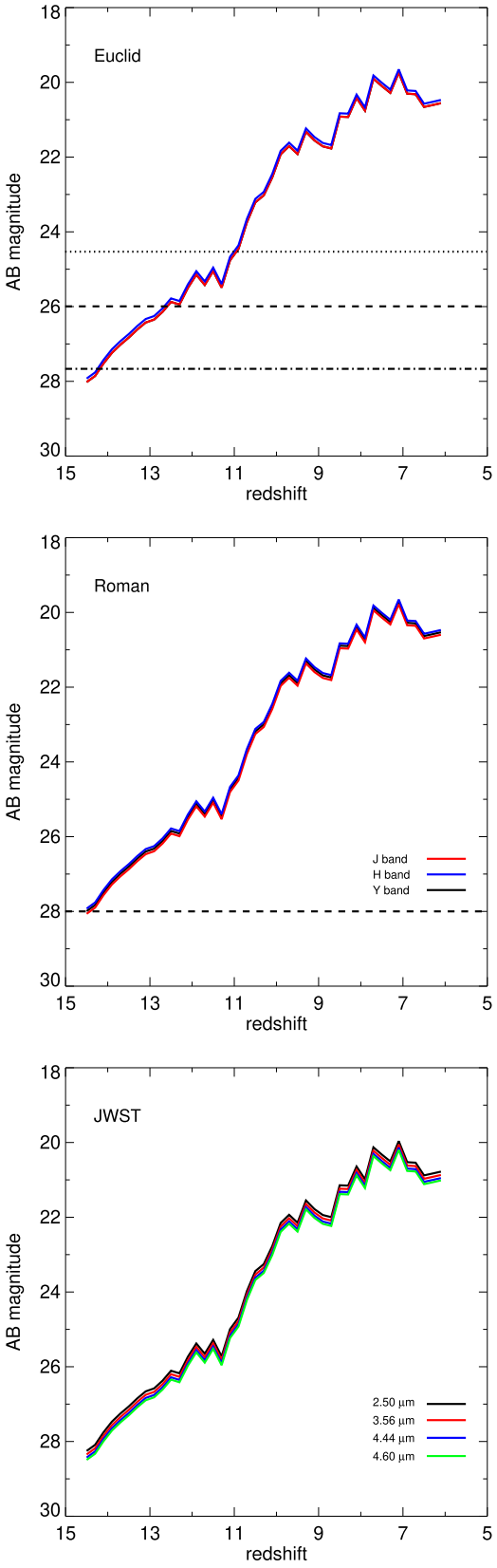

Figure 3. Top: AB magnitudes in Euclid H and J bands. The horizontal dotted, dashed, and dotted–dashed lines are AB mag limits for the Euclid Wide, Deep, and Ultra Deep Surveys, respectively. Center: AB magnitudes in RST H, J, and Y bands. The horizontal dashed line is the AB mag limit for the High Latitude Spectroscopic Survey. Bottom: AB magnitudes in the JWST 2.50 μm, 3.56 μm, 4.44 μm and 4.60 μm NIRCam bands. The JWST NIRCam AB magnitude limit is 32 for these filters, below the scale of the plot.

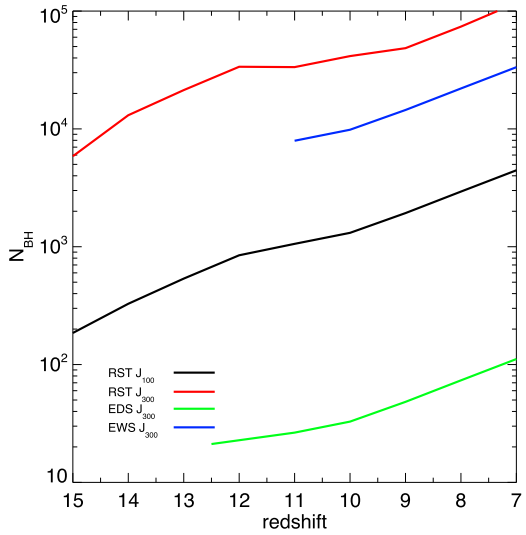

Figure 4. Expected numbers of BH detections in the EW, ED, and HLS surveys based on DCBH number densities from simulations with UV backgrounds of 100 J_{21} and 300 J_{21}, where $J_{21} = 10^{-21}$ erg s^{-1} cm^{-2} Hz^{-1} sr^{-1}. From JWST observations of AGNs that suggest number densities of 10^{-5} Mpc^{-3} at $z = 10$ we expect up to 2000 and 60,000 BHs in the EDS and HLSS at this redshift, respectively.

at $z = 10$, which is on par with those of DCBHs. From simulations we find that RST could detect ∼200–6000 BHs at $z \sim 15$, while the Euclid DS is limited to ∼20 at $z = 12.5$. No detections are expected for the EUDS because its small field (1 deg^2) is too small to enclose any objects, in spite of its high sensitivity. For JWST luminosity functions of 10^{-5} Mpc^{-3} for high-z AGNs (Figure 4 of O. E. Kovács et al. 2024 and Figure 2(a) of K. Inayoshi 2025), the numbers for EDS and HLSS are predicted to be ∼2000 and 60,000, respectively.

For the range of DCBH number densities predicted by simulations, from ∼1000 to 30,000 BHs like UHZ1 or GHZ9 could be found at $z = 10.5$ down to limiting magnitudes of 28 in HLSS, and ∼30 BHs like UHZ1 could be nominally be detected in the EDS at the same redshift at survey depths of 26. Extrapolations of quasar luminosity functions (Euclid Collaboration et al. 2019) predict that Euclid should detect 6–8 quasars at $z > 8$ with magnitudes greater than 23 and that RST should find 180 quasars at $6.5 < z < 9$ and more than 20 at $z > 7.5$ over 2000 deg^2 (W. L. Tee et al. 2023). These numbers are lower than ours because we consider all BHs, not just the most massive ones that become quasars.

We exclude contributions due to stars in the host galaxy in our SMBH spectra but can gauge their effect on AB magnitudes by comparison to P. Natarajan et al. (2024), who include them in their spectral templates for UHZ1. The stars in their synthetic spectra come from analytical fits to an evolving stellar population in a cosmological simulation (B. Agarwal et al. 2014), but they assume the same spectra for the BH as ours, so we can determine the effect of the absence of the host galaxy in our AB magnitudes. They obtain an H-band AB magnitude ∼26.5, which is lower than our ∼23 at the same redshift, but their BH was a factor of 7 lower in mass. When this fact is taken into account the disparity due to stars in the host galaxy is ∼1–1.5 AB mag, which is within the uncertainty of the observed luminosity and does not change our core result. Dust, which has been observed in high-redshift quasars (e.g., R. Maiolino et al. 2004), can also reprocess flux from the BH to longer wavelengths but is subject to radiation pressure that rapidly drives it from the galaxy (e.g., R. Bieri et al. 2017; T. Costa et al. 2018). Nonetheless, the influence of stars and dust in host galaxies of primordial quasars should be quantified in future work.

4. Discussion and Conclusion

RST will have unparalleled sensitivity over large survey areas, so it will be the best bet for initial identification of high-z quasars. It also has seven filters as opposed to Euclid's four for better initial redshift cuts for dropouts. Although RST will perform slitless spectroscopy at 0.8–1.9 μm, the 1 hr exposure required to reach AB mag 28 in the H band will only produce 10σ continuum sensitivity limits of AB mag 21 and 23 for point sources in the prism and grism, respectively, which is insufficient for determination of high redshifts. Consequently, both RST and Euclid will have to rely on efficient photometric techniques such as dropouts or fits of spectral energy distribution templates to the observed photometry with Bayesian methods or neural networks to determine redshifts at high z. The Euclid Collaboration et al. (2019) compared Bayesian and minimal-χ^2/spectral energy distribution fitting methods and found that Bayesian methods, which can reach to at least 0.5 mag fainter, work better than χ^2 fitting methods at lower redshifts ($7 < z < 8$), but at higher redshifts ($z > 8$) they yield similar results (see their Table 3).

However, the accuracy of these techniques can fall off at high redshifts, so JWST or ground-based extremely large telescopes (ELTs) are needed to spectroscopically confirm redshifts for high-z SMBH candidates found by RST and Euclid. JWST is the best telescope for this purpose, given the (sometimes severe) systematics due to atmospheric transmission associated with the ELTs. SKA and ngVLA could also play an important role by confirming the presence of a BH in these candidates at $z \lesssim 14$, especially at 1–10 GHz, where flux from the BH dominates synchrotron emission by supernova remnants in the host galaxy (see Figure 2 in M. A. Latif et al. 2024b).

Euclid, RST, and JWST will for the first time directly probe the the era of SMBH evolution from $z \sim 5$ to 15. Such observations will be key to understanding how populations of early quasars broke off from less massive populations such as AGNs and IMBHs at early redshifts, given the great disparity of their numbers at $z = 6$–7, ∼1 Gpc^{-3} versus a few 10^{-5} Mpc^{-3}. Follow-up observations on these BHs and their host galaxies will yield insights into how feedback from the BH and ionizing UV and supernovae from stars regulated SMBH growth. Exciting new synergies between Euclid, RST, and JWST will inaugurate the era of $z \lesssim 15$ BH astronomy in the coming decade.

Acknowledgments

We thank the anonymous referee for comments that improved this Letter. M.A.L. acknowledges the UAEU for funding via UPAR grant Nos. 31S390 and 12S111.

ORCID iDs

Muhammad A. Latif https://orcid.org/0000-0003-2480-0988
Daniel J. Whalen https://orcid.org/0000-0002-1463-267X

References

Agarwal, B., Dalla Vecchia, C., Johnson, J. L., Khochfar, S., & Paardekooper, J.-P. 2014, MNRAS, 443, 648
Atek, H., Chemerynska, I., Wang, B., et al. 2023, MNRAS, 524, 5486
Bañados, E., Venemans, B. P., Mazzucchelli, C., et al. 2018, Natur, 553, 473
Barrow, K. S. S., Aykutalp, A., & Wise, J. H. 2018, NatAs, 2, 987
Bieri, R., Dubois, Y., Rosdahl, J., et al. 2017, MNRAS, 464, 1854
Bogdán, Á., Goulding, A., Natarajan, P., et al. 2024, NatAs, 8, 126
Bunker, A. J., Saxena, A., Cameron, A. J., et al. 2023, A&A, 677, A88
Castellano, M., Fontana, A., Treu, T., et al. 2023, ApJL, 948, L14
Costa, T., Rosdahl, J., Sijacki, D., & Haehnelt, M. G. 2018, MNRAS, 473, 4197
Di Matteo, T., Croft, R. A. C., Feng, Y., Waters, D., & Wilkins, S. 2017, MNRAS, 467, 4243
Di Matteo, T., Khandai, N., DeGraf, C., et al. 2012, ApJL, 745, L29
Euclid Collaboration, Barnett, R., Warren, S. J., et al. 2019, A&A, 631, A85
Euclid Collaboration, Mellier, Y., Abdurro'uf, et al. 2025, A&A, 697, A1
Fan, X., Strauss, M. A., Schneider, D. P., et al. 2003, AJ, 125, 1649
Goulding, A. D., Greene, J. E., Setton, D. J., et al. 2023, ApJL, 955, L24
Habouzit, M., Volonteri, M., Latif, M., Dubois, Y., & Peirani, S. 2016, MNRAS, 463, 529
Haemmerlé, L., Woods, T. E., Klessen, R. S., Heger, A., & Whalen, D. J. 2018, MNRAS, 474, 2757
Herrington, N. P., Whalen, D. J., & Woods, T. E. 2023, MNRAS, 521, 463
Hosokawa, T., Yorke, H. W., Inayoshi, K., Omukai, K., & Yoshida, N. 2013, ApJ, 778, 178
Inayoshi, K. 2025, ApJL, 988, L22
Inayoshi, K., Haiman, Z., & Ostriker, J. P. 2016, MNRAS, 459, 3738
Ji, X., Übler, H., Maiolino, R., et al. 2024, MNRAS, 535, 881
Kitayama, T., Yoshida, N., Susa, H., & Umemura, M. 2004, ApJ, 613, 631
Kocevski, D. D., Finkelstein, S. L., Barro, G., et al. 2025, ApJ, 986, 126
Kokorev, V., Caputi, K. I., Greene, J. E., et al. 2024, ApJ, 968, 38
Kovács, O. E., Bogdán, Á., Natarajan, P., et al. 2024, ApJL, 965, L21
Larson, R. L., Finkelstein, S. L., Kocevski, D. D., et al. 2023, ApJL, 953, L29
Latif, M. A., Aftab, A., & Whalen, D. J. 2024a, AJ, 167, 251
Latif, M. A., Aftab, A., Whalen, D. J., & Mezcua, M. 2025, A&A, 694, L14
Latif, M. A., Khochfar, S., Schleicher, D., & Whalen, D. J. 2021, MNRAS, 508, 1756
Latif, M. A., Whalen, D., & Khochfar, S. 2022a, ApJ, 925, 28
Latif, M. A., & Whalen, D. J. 2025, MNRAS, 537, 3448
Latif, M. A., Whalen, D. J., Khochfar, S., Herrington, N. P., & Woods, T. E. 2022b, Natur, 607, 48
Latif, M. A., Whalen, D. J., & Mezcua, M. 2024b, MNRAS, 527, L37
Lupi, A., Haiman, Z., & Volonteri, M. 2021, MNRAS, 503, 5046
Lupi, A., Quadri, G., Volonteri, M., Colpi, M., & Regan, J. A. 2024, A&A, 686, A256
Maiolino, R., Schneider, R., Oliva, E., et al. 2004, Natur, 431, 533
Makishima, K., Kubota, A., Mizuno, T., et al. 2000, ApJ, 535, 632
Mortlock, D. J., Warren, S. J., Venemans, B. P., et al. 2011, Natur, 474, 616
Nagele, C., Umeda, H., & Takahashi, K. 2023a, MNRAS, 523, 1629
Nagele, C., Umeda, H., Takahashi, K., & Maeda, K. 2023b, MNRAS, 520, L72
Nandal, D., Regan, J. A., Woods, T. E., et al. 2024a, A&A, 683, A156
Nandal, D., Whalen, D. J., Latif, M. A., & Heger, A. 2025, arXiv:2502.04435
Nandal, D., Zwick, L., Whalen, D. J., et al. 2024b, A&A, 689, A351
Natarajan, P., Pacucci, F., Ferrara, A., et al. 2017, ApJ, 838, 117
Natarajan, P., Pacucci, F., Ricarte, A., et al. 2024, ApJL, 960, L1
O'Brennan, H., Regan, J. A., Brennan, J., et al. 2025, OJAp, 8, 88
Patrick, S. J., Whalen, D. J., Latif, M. A., & Elford, J. S. 2023, MNRAS, 522, 3795
Salvaterra, R., Haardt, F., & Ferrara, A. 2005, MNRAS, 362, L50
Sazonov, S. Y., Ostriker, J. P., & Sunyaev, R. A. 2004, MNRAS, 347, 144
Senchyna, P., Plat, A., Stark, D. P., et al. 2024, ApJ, 966, 92
Smidt, J., Whalen, D. J., Johnson, J. L., Surace, M., & Li, H. 2018, ApJ, 865, 126
Smith, B. D., Regan, J. A., Downes, T. P., et al. 2018, MNRAS, 480, 3762
Surace, M., Zackrisson, E., Whalen, D. J., et al. 2019, MNRAS, 488, 3995
Surace, M., Whalen, D. J., Hartwig, T., et al. 2018, ApJL, 869, L39
Tee, W. L., Fan, X., Wang, F., et al. 2023, ApJ, 956, 52
Tenneti, A., Di Matteo, T., Croft, R., Garcia, T., & Feng, Y. 2018, MNRAS, 474, 597
Valentini, M., Gallerani, S., & Ferrara, A. 2021, MNRAS, 507, 1
Vikaeus, A., Whalen, D. J., & Zackrisson, E. 2022, ApJL, 933, L8
Volonteri, M., Silk, J., & Dubus, G. 2015, ApJ, 804, 148
Wang, F., Yang, J., Fan, X., et al. 2021, ApJL, 907, L1
Wang, Y., Zhai, Z., Alavi, A., et al. 2022, ApJ, 928, 1
Whalen, D., Abel, T., & Norman, M. L. 2004, ApJ, 610, 14
Whalen, D. J., & Fryer, C. L. 2012, ApJL, 756, L19
Whalen, D. J., Latif, M. A., & Mezcua, M. 2023, ApJ, 956, 133
Whalen, D. J., Mezcua, M., Meiksin, A., Hartwig, T., & Latif, M. A. 2020a, ApJL, 896, L45
Whalen, D. J., Mezcua, M., Patrick, S. J., Meiksin, A., & Latif, M. A. 2021, ApJL, 922, L39
Whalen, D. J., Surace, M., Bernhardt, C., et al. 2020b, ApJL, 897, L16
Woods, T. E., Heger, A., Whalen, D. J., Haemmerlé, L., & Klessen, R. S. 2017, ApJL, 842, L6
Woods, T. E., Patrick, S., Elford, J. S., Whalen, D. J., & Heger, A. 2021, ApJ, 915, 110
Woods, T. E., Agarwal, B., Bromm, V., et al. 2019, PASA, 36, e027
Yang, J., Wang, F., Fan, X., et al. 2020, ApJL, 897, L14
Yue, B., Ferrara, A., Salvaterra, R., Xu, Y., & Chen, X. 2013, MNRAS, 433, 1556